https://doi.org/10.3311/PPch.40264

Periodica Polytechnica Chemical Engineering, 69(3), pp. 385–402, 2025

Improvement of Effectiveness and Photocatalytic Properties of Poly(vinylidene Fluoride)-TiO_2-WO_3 Membrane with Polydopamine Modification for Natural Rubber Wastewater Treatment

Tutuk Djoko Kusworo[1*], Zahra Maharani Wilukindra[1], Muhammad Ammar Atthoriq[1], Meitri Bella Puspa[1], Muhammad Itsar Hanif[1], Dani Puji Utomo[1]

[1] Department of Chemical Engineering, Faculty of Engineering, Diponegoro University, Jl. Prof. Soedarto No. 13, 50275 Semarang, Central Java, Indonesia
[*] Corresponding author, e-mail: tdkusworo@che.undip.ac.id

Received: 21 February 2025, Accepted: 01 August 2025, Published online: 08 September 2025

Abstract

This study investigates the enhancement of poly(vinylidene fluoride) (PVDF) membranes modified with TiO_2, tungsten trioxide, and coated with polydopamine (PDA) for rubber industry wastewater treatment. PDA coating improved the adhesion and dispersion of photocatalyst particles on the PVDF membrane. Membrane characterization using FTIR, SEM, SEM-EDX, XRD, mechanical strength, porosity, pore size analysis, water contact angle, and water uptake confirmed the structural and surface property enhancements of the PVDF-TiO_2-WO_3/PDA membrane, which contributed to improved pollutant rejection performance. The PVDF-TiO_2-WO_3/PDA membrane enhanced ammonia, phenol, chemical oxygen demand, and total dissolved solids rejection by 98.22%, 99.39%, 87.18%, and 51.06%, respectively, compared to the pristine PVDF membrane. After pretreatment, the flux value was 154.32 L/m^2·h. The membrane exhibited the best photocatalytic degradation activity, with TiO_2-WO_3 nanoparticles enhancing pollutant removal under visible light and PDA coating contributing to enhanced selective permeability. Kinetic studies indicated that the zero-order kinetic model best describes photocatalytic activity. Membrane performance remained stable over five cycles, with high pollutant rejection despite some pore blockage and swelling. Overall, PDA modification on PVDF-TiO_2-WO_3 membranes offers a promising solution for efficient and environmentally friendly rubber wastewater treatment.

Keywords

rubber waste, photocatalysis, TiO_2, WO_3, PDA

1 Introduction

The sustainable management of industrial wastewater is crucial to achieving several of the United Nations Sustainable Development Goals (SDG), particularly SDG 6 (Clean Water and Sanitation) and SDG 12 (Responsible Consumption and Production) [1]. With rapid industrialization, wastewater treatment has become an urgent challenge, especially in industries producing large volumes of effluent that can significantly impact water quality, ecosystems, and public health. Indonesia, one of the largest natural rubber (NR) producers globally, faces considerable difficulties in effectively managing the effluents generated during rubber processing. Currently, 115 rubber industries are operating in Indonesia, collectively producing over 12 million tonnes of NR annually, which is utilized in various commercial products such as gloves, tyres, balloons, rubber shoes, mattresses, swimming caps, catheters, and bottle cap [2]. However, rubber manufacturing companies produce a significant quantity of waste annually. Each Indonesian rubber sector typically generates 300–400 m^3 of effluent daily [3]. High concentrations of chemical oxygen demand (COD) (187,432.1 mg/L), pH (4.23), total nitrogen (1,157.1 mg/L), ammonia nitrogen (1,113.0 mg/L), total phosphorus (1,181.2 mg/L), zinc (593.3 mg/L), chromium (0.6127 mg/L), and nickel (0.2986 mg/L) [4] in untreated rubber processing wastewater pose a significant risk of environmental degradation. Inadequate treatment and improper disposal of such waste can result in water contamination, threatening aquatic ecosystems and endangering

Cite this article as: Kusworo, T. D., Wilukindra, Z. M., Atthoriq, M. A., Bella Puspa, M., Hanif, M. I., Puji Utomo, D. "Improvement of Effectiveness and Photocatalytic Properties of Poly(vinylidene Fluoride)-TiO_2-WO_3 Membrane with Polydopamine Modification for Natural Rubber Wastewater Treatment", Periodica Polytechnica Chemical Engineering, 69(3), pp. 385–402, 2025. https://doi.org/10.3311/PPch.40264

human populations reliant on water resources. Addressing the treatment of rubber industry wastewater is, therefore, essential for maintaining water quality and ensuring sustainable industrial practices that align with SDG 6.

The use of ozonation for wastewater treatment has gained attention due to its ability to degrade pollutants efficiently [5]. However, ozonation can cause significant damage to biopolymers, reducing the effectiveness of ultrafiltration (UF) and microfiltration (MF) membranes by contributing to flux decline and membrane fouling [6]. This drawback necessitates exploring alternative or complementary treatment methods to mitigate membrane fouling and enhance wastewater treatment. One such method is adsorption, where pollutants are removed through their accumulation on adsorbent surfaces [7]. Adsorption is an effective and low-cost process that can be particularly useful when combined with other treatment techniques [8]. Consequently, integrating ozonation [9], adsorption [10], and membrane filtration [11] has emerged as a highly promising strategy for the effective treatment of rubber wastewater. Membrane technology has become a prominent solution for wastewater treatment due to its many advantages, including low energy consumption, ease of operation, minimal land area requirements, and environmental sustainability [12]. The versatility of membrane filtration is further enhanced when combined with photocatalytic degradation, a process known for its efficiency, low cost, and environmental benefits. Photocatalysis has emerged as an effective method to degrade harmful pollutants, making it particularly suitable for water treatment applications [13]. In this study, a novel approach to rubber wastewater treatment is explored using poly(vinylidene fluoride) (PVDF) membranes modified with TiO_2 and WO_3, incorporating polydopamine (PDA) as a coating. This combination is expected to improve membrane performance and photocatalytic properties, thus enhancing the overall treatment efficiency.

PVDF resistance to oxidative degradation, its thermal and hydrolytic stability, and superior mechanical strength ensure its durability and reliability in harsh industrial conditions. These properties make it indispensable for advanced membrane development, especially when modified with nanomaterials to enhance hydrophilicity, antifouling, and pollutant rejection [14]. The incorporation of photocatalytic materials into membrane systems has gained attention for enhancing membrane performance and functionality. TiO_2 is widely used for its high photocatalytic activity, chemical stability, and environmental safety. However, its wide bandgap (3.2 eV) limits activation to UV light, which represents only ~5% of solar radiation, necessitating strategies to extend its activity into the visible light spectrum [15]. Blending TiO_2 with WO_3, a visible-light-active photocatalyst with a narrower bandgap (2.4–2.8 eV), is a promising solution. WO_3 offers strong oxidative potential, photostability, and resistance to photo-corrosion [16]. The TiO_2/WO_3 combination enhances light absorption, improves charge separation by reducing electron-hole recombination, and achieves superior photocatalytic performance compared to either material alone. Incorporating TiO_2/WO_3 composites into membranes also improves hydrophilicity, antifouling properties, and pollutant rejection. In addition to the photocatalytic materials, PDA has shown great potential as a membrane modifier. PDA is known for its high hydrophilicity, which can improve membrane properties by enhancing water flux and reducing fouling [17].

The primary objective of this study is to evaluate the effects of TiO_2/WO_3 concentration in PVDF-TiO_2-WO_3 nanohybrid membranes on membrane characteristics and performance for the treatment of rubber wastewater. Bentonite was incorporated as a pretreatment adsorbent due to its high surface area and cation exchange capacity, which enable effective adsorption of various organic contaminants prior to membrane photocatalytic treatment. The study also aims to assess the impact of ozone pretreatment and bentonite adsorption on membrane fouling mitigation and overall performance. Furthermore, the effect of PDA coating on the properties of PVDF-TiO_2-WO_3 membranes will be explored, as well as the photocatalytic kinetics in the treatment of rubber effluent. By investigating these factors, this research aims to contribute to the development of more efficient, sustainable, and cost-effective methods for treating industrial wastewater, specifically in the rubber industry, thus supporting global efforts toward clean water and responsible industrial practices.

2 Materials and methods

2.1 Materials

The materials and reagents used in this research included rubber waste liquid, PVDF (SOLEF 6020/1001, 99%) with M_n = 153 g/mol, M_w = 352 g/mol, nano material TiO_2 were supplied by Nano Center Indonesia. WO_3 (99%) and N-methyl-2-pyrrolidone (NMP, 99%) were purchased from Merck, Germany, and used as a solvent. Sigma-Aldrich provided dopamine hydrochloride and tris(hydroxymethyl)amino-methane hydrochloride (Tris-HCl,

99.8%). Bentonite, an adsorption pretreatment agent for contaminant removal in rubber wastewater, was supplied by Brataco Chemika, Indonesia. $K_2Cr_2O_7$, H_2SO_4, ferro ammonium sulfate (FAS), potassium hydrogen phthalate (KHP), and deionized water for phase inversion were obtained from Indrasari, Local Chemical Indonesian. Bentonite clay granule was supplied by Brataco Chemika, Indonesia. All the materials used in this research were of analytical grade and applied as received. The NR wastewater as feed was obtained from Bengkulu, Indonesia.

2.2 Fabrication of PDA-coated PVDF-TiO_2-WO_3 membrane

The fabrication of composite membranes composed of PVDF, TiO_2, WO_3, and PDA is summarized in Table 1. The membranes were prepared using a combination of the dry-wet phase inversion technique and the dip-coating method to achieve optimal structural and functional properties [18]. The fabrication process commenced with the preparation of a 15% (m/v) PVDF polymer solution by dissolving PVDF granules in NMP under continuous stirring at 60–70 °C for 12 h to ensure complete dissolution. Simultaneously, TiO_2 and WO_3 nanoparticles were dispersed in the same solvent through ultrasonication at 20 kHz for 1 h to achieve uniform dispersion and prevent nanoparticle agglomeration. The nanoparticle suspension was then gradually added to the polymer solution under constant stirring to produce a homogeneous casting solution. The casting solution was spread onto clean glass plates to form membranes with a thickness of approximately 150 μm, using a casting knife for uniformity. To remove entrapped air bubbles, the solution was left undisturbed for 24 h at ambient temperature. The cast film was then immersed in deionized water for 24 h to induce phase separation, leading to the formation of a porous membrane structure. Following phase separation, the membranes were transferred to a coagulation bath containing distilled water, where they were soaked for an additional 24 h at room temperature to enhance residual solvent removal and improve membrane structural integrity. Finally, the membranes were air-dried at 30 °C for 24 h.

Table 1 Composition of fabricated membranes

Membrane	NMP (wt%)	PVDF (wt%)	TiO_2 (wt%)	WO_3 (wt%)	TiO_2/WO_3 (wt%)	PDA (wt%)
M-01	85	15	-	-	-	-
M-02	85	15	1	-	-	-
M-03	85	15	-	1.5	-	-
M-04	85	15	-	-	1/1.5	-
M-05	85	15	-	-	1/1.5	0.5
M-06	85	15	-	-	1/1.5	1
M-07	85	15	-	-	1/1.5	1.5

2.3 Characterization of PVDF-TiO_2-WO_3/PDA membrane

The morphological features of the fabricated membranes were examined using a scanning electron microscope (SEM, JEOL Series JSM-6510-LA, Japan) coupled with energy-dispersive X-ray (EDX) spectroscopy for elemental composition and mapping analysis. The phase crystallinity of the materials was determined via X-ray diffraction (XRD, SHIMADZU XRD-7000, Japan). The hydrophilicity of the membranes was evaluated using a contact angle goniometer (OCA25, Dataphysics Instruments, Germany) to determine both the static contact angle and surface energy.

2.4 Membrane performance evaluation

The performance of the synthesized membranes was evaluated based on their permeability and ability to remove COD, phenol, and NH_3-N during wastewater treatment via photofiltration. The parameters were determined at room temperature (30 °C). The assessment focused on permeate flow rates and pollutant COD, phenol, and NH_3-N using NR as the feed. Before filtration, the membranes were compacted with demineralized water at 5 bar for 30 min. The system was then operated at 5 bar, with an effective membrane area of $1.26 \cdot 10^{-3}$ m^2. Permeate samples were collected every 30 min, and water flux was calculated using Eq. (1).

$$J = \frac{\Delta V}{S \cdot \Delta t} \tag{1}$$

In Eq. (1), J represents the flux value ($L/m^2 \cdot h$), ΔV represents the total volume of the permeate (L) collected during the operation time Δt (h), and S represents the membrane effective area for filtration (m^2).

In assessing contaminant rejection, the concentrations of COD, phenol, and NH_3-N were quantified using a Thermo Scientific Genesys 10s UV-Vis Spectrophotometer (Thermo Electron Scientific Instruments LLC., Madison, WI, USA). The rejection value of the membrane can be calculated using Eq. (2):

$$R_E = \left(1 - \frac{C_t}{C_0}\right) \cdot 100\% \tag{2}$$

where R_E is the pollutant removal efficiency (%), whereas C_t and C_0 are the concentration of the contaminant in permeate and feed, respectively.

2.5 The photocatalytic activity of PVDF-TiO_2-WO_3/PDA nanohybrid membranes

The photocatalytic activity test of PVDF-TiO_2-WO_3/PDA nanohybrid membranes are based on procedures that refer to research conducted by Kusworo et al. [19], by evaluating the rate of organic degradation indicated by a decrease of rejection values in rubber wastewater. The membrane is mounted on a glass slide and then inserted into a container containing rubber wastewater and allowed to stand in a dark environment for 60 min to start adsorption and ensure only photocatalytic activity will be tested. The experiment was conducted in a batch reactor system for 120 min and every 30 min samples were taken from the reactor for rejection testing. The photocatalytic degradation kinetics of the fabricated photocatalytic membrane composites were further analyzed using the zero-order, pseudo-first-order, and modified Freundlich kinetic models. The mathematical formulations for these models are provided in Eqs. (3), (4), and (5), respectively.

$$C_0 - C_t = k_0 t \tag{3}$$

$$\ln\left(\frac{C_0}{C_t}\right) = k_1 t \tag{4}$$

$$C_t = k_F C_0 t^{\frac{1}{m}} \tag{5}$$

The k_0 (mg/L·min), k_1 (1/min), and k_F (1/min) represent the rate constants for the zero-order, pseudo-first-order, and modified Freundlich kinetic models, respectively, while t stands for time (min). The m represent dimensionless heterogeneity factor in the modified Freundlich model.

2.6 Reusability and stability of PVDF-TiO_2-WO_3/PDA nanohybrid membranes

To assess the stability and reusability of the membranes, a series of experiments were conducted over five consecutive cycles to evaluate permeate flux and pollutant removal efficiency. Each cycle involved 120 min of produced water filtration, with permeate flux and pollutant removal rates measured at 30 min intervals to track the membrane performance over time. Before each subsequent cycle, the membrane was thoroughly cleaned with demineralized water to remove any fouling or contaminants, ensuring the membrane's optimal performance was maintained throughout the experiment. This cleaning procedure was crucial in evaluating the membrane's ability to retain its effectiveness after each cycle. The structured testing approach provided detailed insights into the membrane's stability, performance consistency, and capacity to recover its filtration properties after cleaning. The results of these multi-cycle experiments offer a comprehensive assessment of the membrane's long-term durability, operational efficiency, and suitability for continuous use in real-world applications, such as wastewater treatment, where long-term performance and ease of cleaning are essential for practical implementation.

3 Results and discussion

3.1 Characteristics of the NR wastewater

The water quality index (WQI) analysis in Table 2 yielded a value of 83.188, classifying the water quality as poor and underscoring the need for improvement across several parameters. The evaluated parameters include pH, total dissolved solids (TDS), COD, ammonia, and phenol key indicators of industrial wastewater pollution, particularly from NR treatment [20]. The pH 8.2, slightly alkaline, contributed 3.856 to the WQI. Although within acceptable regulatory limits (pH 6–9) set by local and international standards, pH levels exceeding 8.5 may indicate the presence of alkaline detergents or processing chemicals, warranting stabilization measures. The TDS concentration 421 mg/L contributed 0.263 to the WQI, indicating elevated dissolved solids, likely derived from residual chemicals and salts used in rubber coagulation. Such levels pose risks to freshwater ecosystems, necessitating treatment to meet discharge thresholds, typically around 500 mg/L. The COD level 91.755 mg/L, contributing 1.176 to the WQI, signifies substantial organic contamination, which may deplete dissolved oxygen in receiving waters. This value is nearing the upper regulatory threshold (50–100 mg/L), underscoring the necessity for additional treatment to reduce the organic load. Ammonia, measured

Table 2 WQI of NR wastewater in Bengkulu, Indonesia

Parameters*	*Sn*	1/*Sn*	*W* = *K*/*Sn*	*Qn* = (*Vn*/*Sn*)·100	*Wm*·*Qn*
pH	8.2	0.122	0.136	28.333	3.856
TDS	421	0.002	0.003	99.287	0.263
COD	91.755	0.011	0.012	96.670	1.176
Ammonia	1.32	0.758	0.846	91.667	77.505
Phenol	278.58	0.004	0.004	96.669	0.387
Total		0.896	1		83.188

* The parameters were determined at room temperature (30 °C).
Sn: standard permissible value for parameter *n*,
W: unit weight of parameter *n* in the WQI calculation,
K: proportionality constant for assigning unit weights in WQI,
Vn: observed value of parameter *n* in the water sample,
Qn: quality rating scale for parameter *n*,
Wm: weighted quality rating of parameter *n*.

as 1.32 mg/L, accounted for the highest contribution to the WQI, 77.505. As a byproduct of nitrogen-based compounds in rubber processing, ammonia concentrations exceeding 1 mg/L pose a significant threat to aquatic ecosystems, necessitating advanced treatment methods such as nitrification or stripping. Phenol, with a concentration 278.58 μg/L, contributed 0.387 to the WQI. While its level remains below regulatory limits, phenol is a toxic pollutant that requires further mitigation. In conclusion, the WQI value of 83.188 reflects marginally acceptable water quality, yet parameters such as ammonia, COD, and TDS exceed permissible thresholds and demand targeted improvements. To enhance water quality and ensure compliance with environmental regulations, comprehensive treatment strategies combining physical, chemical, and biological methods are strongly recommended.

3.2 Characterization of membrane TiO_2/WO_3

3.2.1 SEM EDX analysis for elemental composition and distribution

The SEM-EDX analysis of M-07 membrane provides valuable insights into its elemental composition, offering key information about its surface characteristics and potential performance in filtration applications. As confirmed by the SEM image in Fig. 1 (a), the membrane surface exhibits a well-integrated structure, with TiO_2 and WO_3 nanoparticles dispersed within the PVDF matrix. The overlay of TiO_2-WO_3/PDA distribution in Fig. 1 (b) further illustrates the uniform distribution of these components across the membrane surface. Table 3 shows the elemental analysis revealing that the membrane is predominantly composed of carbon (47.82% m/m) and fluorine (43.85% m/m), which are attributed to the PVDF matrix and contribute to the membrane hydrophobicity and chemical stability. Oxygen (2.23% m/m) is also present, primarily as part of the TiO_2 and WO_3, which are essential to the composite structure. This proves the successful incorporation of TiO_2 and WO_3 into the PVDF membrane. The presence of oxygen in the membrane identifies an increase in membrane hydrophilicity due to the high affinity of oxygen-containing compounds to water [21]. The distribution of fluorine shown in Fig. 1 (c) and titanium in Fig. 1 (d) clearly indicates that these elements are embedded within the membrane, confirming the presence of the PVDF matrix and TiO_2 nanoparticles. The distribution of tungsten shown in Fig. 1 (e) further verifies the incorporation of WO_3 nanoparticles, which enhance the membrane's photocatalytic properties. The presence of titanium (1.38% m/m) and tungsten (3.97% m/m) suggests that TiO_2 and WO_3 nanoparticles are integrated into the membrane. They are known for their photocatalytic properties that improve the membrane's ability to degrade organic contaminants, particularly under light irradiation. Trace elements, such as thallium, aluminum, and copper, were also detected in minimal amounts, indicating that these elements may be impurities or byproducts from the synthesis process, as reflected in the EDX spectrum shown in Fig. 1 (f). The compound analysis further confirms the dominance of carbon and fluorine from the PVDF matrix, while TiO_2 and WO_3 are identified as key photocatalytic components. Overall, the SEM-EDX analysis demonstrates that the PVDF-TiO_2-WO_3/PDA membrane possesses a well-integrated structure with significant photocatalytic functionality, making it a promising candidate for advanced filtration applications where fouling resistance and photocatalytic degradation are critical.

3.2.2 XRD analysis of fabricated membranes

In Fig. 2, the XRD analysis of the PVDF-TiO_2-WO_3/PDA membrane is presented. Phase identification was performed by detecting diffraction peaks corresponding to several crystalline phases, namely TiO_2, WO_3, PDA, and PVDF, which contribute to the overall properties of the membrane. Diffraction peaks at 2θ 25.3°, 27.39°, 34.28°, 36.17°, 43.67°, and 54.51° correspond to the anatase phase of TiO_2, known for its high photocatalytic activity. The most prominent peak at 25.3° corresponds to the (101) crystal plane of anatase TiO_2 [22], while the peaks at 27.39° and 36.17° correspond to the (002) and (101) planes, respectively [23]. The high intensity of these peaks indicates the dominant presence of the anatase phase, which is highly beneficial for photocatalytic applications due to its efficient charge transfer capabilities [24]. In addition to TiO_2, the XRD pattern also reveals diffraction peaks at 22.47°, 33.42°, 50.33°, and 56.8°, associated with the WO_3 phase, confirming the incorporation of WO_3 into the membrane matrix. WO_3 is well known for its photocatalytic properties, and its presence in the membrane can enhance photocatalytic efficiency, particularly under visible light irradiation. These peaks can be indexed to the WO_3 crystal planes using Miller indices, namely (001) at 22.47°, (110) at 33.42°, (200) at 50.33°, and (220) at 56.8°, indicating specific crystal orientations within the WO_3 structure. The presence of these peaks suggests successful crystallization of WO_3, contributing to the enhancement of the membrane's photocatalytic efficiency. The XRD analysis further revealed characteristic "bread" peaks of PDA, along with unique diffraction peaks between 20° and 27°,

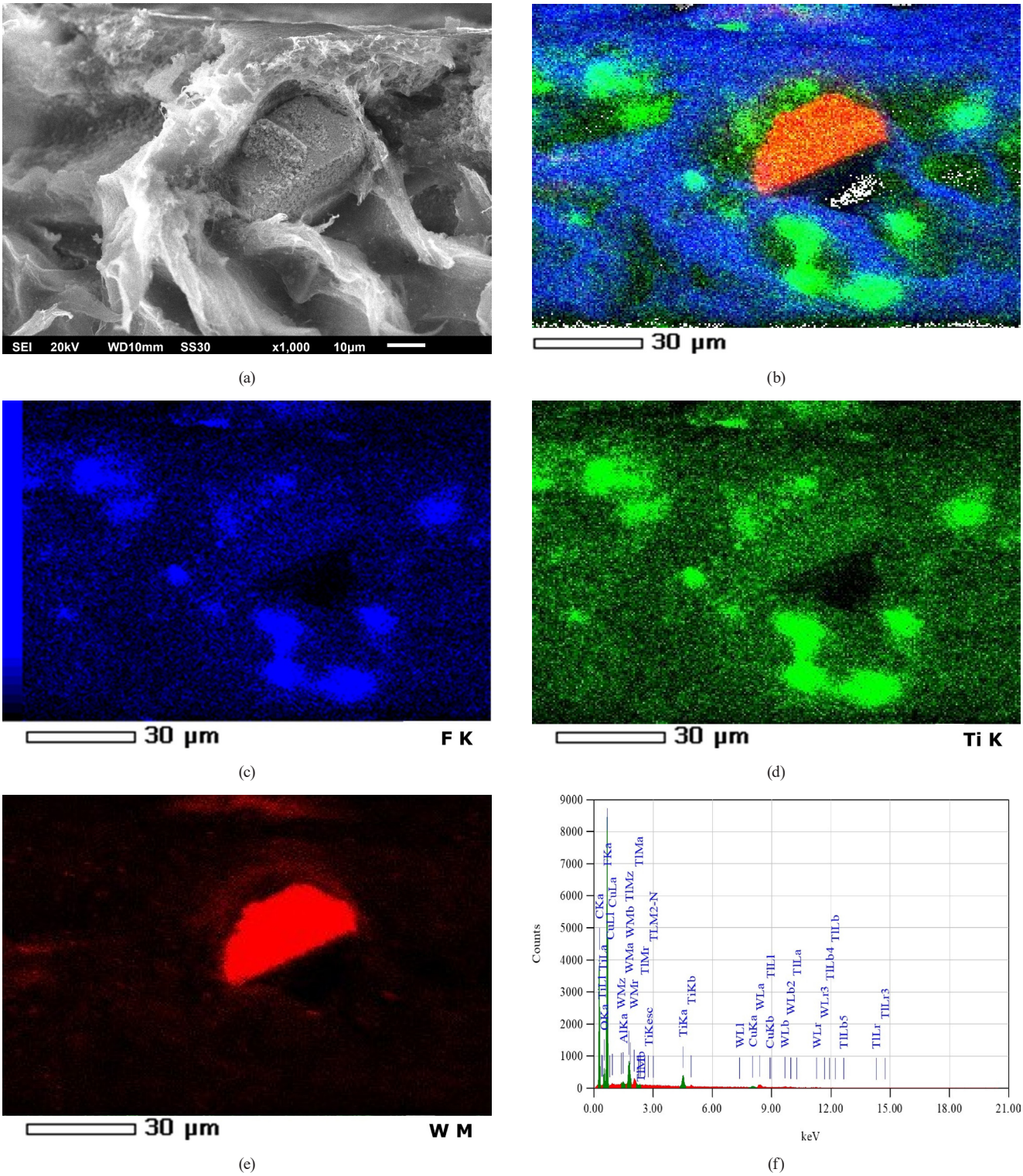

(a) (b) (c) (d) (e) (f)

Fig. 1 (a) SEM image, (b) overlay of TiO_2-WO_3/PDA distribution, (c) fluorine distribution, (d) titanium distribution, (e) tungsten distribution, (f) EDX spectrum of M-07 membrane

indicating the successful incorporation of PDA into the membrane surface. PDA plays a crucial role in enhancing the hydrophilicity and antimicrobial properties of the membrane, which are vital for improving long-term filtration performance [25]. Moreover, the emergence of the β-phase of PVDF in the XRD analysis was also detected, with a diffraction peak at 20.99°, indicating a phase transition from the α-phase of PVDF. The β-phase exhibits higher polarity compared to the α-phase, which can enhance interactions with water and improve the hydrophilicity of the membrane. The presence of the β-phase PVDF is expected to improve the membrane's filtration

Table 3 Elemental and oxide composition analysis for M-07 using EDX

Elementals	Mass %	Atomic %	Compound	Mass %	Atomic %
C	47.82	58.39	C	47.92	49.433
O	2.23	5.38		-	-
F	43.85	35.28	F	43.85	38.22
Ti	1.38	0.42	TiO_2	2.30	3.22
W	3.97	0.32	WO_3	5.0	7.36
Tl	0.01	0.00	Tl_2O_3	0.01	0.02
Al	0.13	0.04	Al_2O_3	0.24	0.207
Cu	0.62	0.15	CuO	0.77	1.36
Total	100.00	100.00		100.0	100.00

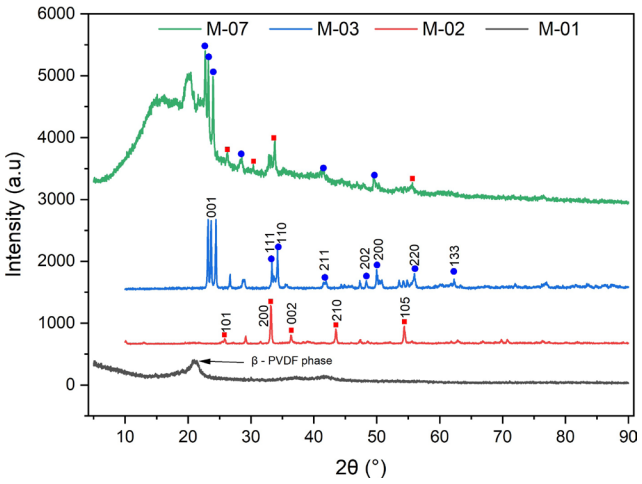

Fig. 2 XRD diffractogram of the membranes

performance by reducing water rejection coefficients and enhancing its fouling resistance [26]. Overall, the XRD results reveal well-ordered crystalline structures for TiO_2, WO_3, and PVDF, with characteristic peaks for each phase. The synergistic combination of TiO_2, which possesses high photocatalytic activity, WO_3, which also contributes to photocatalytic degradation, and the *β*-phase PVDF, which enhances hydrophilicity, collectively improves the photocatalytic and filtration performance of the membrane. The addition of PDA further enhances the surface properties of the membrane, increasing resistance to fouling and improving hydrophilicity, making it more suitable for advanced water filtration and purification applications.

3.2.3 Water contact angle and water uptake ability

Table 4 presents the water contact angle and absorption capacity of the fabricated membranes, reflecting their surface affinity for water and moisture absorption. The contact angle indicates the membrane's hydrophobicity or hydrophilicity, with lower values signaling increased hydrophilicity. Membrane M-01, with a higher contact angle (87.80°), exhibits stronger hydrophobicity and

Table 4 Water contact angle and water uptake ability fabricated membranes

Membrane	Contact angle (°)	W_d	W_w	Water uptake ability (m/m)
M-01	87.80	0.024	0.045	46.66
M-02	76.80	0.0150	0.073	79.45
M-03	84.40	0.0180	0.072	75.00
M-04	73.20	0.0130	0.080	83.75
M-05	70.61	0.0128	0.082	84.35
M-06	67.93	0.0129	0.084	85.65
M-07	62.60	0.0110	0.086	89.90

a lower absorption capacity (46.66%), making it less efficient at absorbing water. In contrast, Membrane M-02, with a lower contact angle (76.80°) and higher absorption (79.45%), demonstrates enhanced hydrophilicity, improving its ability to absorb and drain water. The addition of TiO_2 in M-02 contributes to its hydrophilic properties by reducing the contact angle and increasing water absorption, thereby enhancing its filtration efficiency. Membrane M-03, with a contact angle of 84.40° and a water absorption capacity of 75.00%, exhibits intermediate hydrophilicity. The incorporation of WO_3 into the membrane matrix resulted in only a marginal enhancement of hydrophilic properties, indicating that the full potential of WO_3 in improving surface wettability was not effectively harnessed [27]. This suboptimal performance is plausibly attributed to the heterogeneous distribution and partial agglomeration of WO_3 nanoparticles within the polymeric framework, as illustrated in the SEM micrograph (Fig. 1 (e)). Such morphological inhomogeneities likely restrict the availability of surface-exposed hydroxyl functionalities, which play a pivotal role in facilitating water–surface interactions. Furthermore, if the introduction of WO_3 predominantly increases the surface roughness without a corresponding augmentation in surface energy, the membrane may exhibit elevated contact angles. This phenomenon is consistent with theoretical interpretations provided by the Wenzel and Cassie–Baxter models, wherein the entrapment of air within surface asperities can impede effective wetting [28]. In addition, the relatively low WO_3 content employed in the M-03 formulation may be inadequate to induce a significant transformation in surface chemical characteristics, particularly when the host polymer is intrinsically hydrophobic. Consequently, the inherent interfacial properties of the base material may dominate over the hydrophilic contributions of the additive, thereby mitigating the expected decrease in water contact angle. Membrane M-04, with a water contact angle of 73.20° and a high water absorption capacity (83.75%),

is more hydrophilic than M-01 and M-02, offering potential benefits for filtration and separation applications. However, it lacks photocatalytic materials, limiting its photodegradation capabilities. Membrane M-07, with the lowest contact angle (62.60°) and the highest water absorption capacity (86.90%), is the most hydrophilic. The PDA coating enhances its hydrophilicity, improving water absorption and interaction [29]. FTIR analysis confirms the presence of hydrophilic groups, such as −OH groups from TiO_2 and WO_3, which further strengthen the membrane affinity for water [30]. The PDA coating, combined with TiO_2 and WO_3, optimizes the membrane's hydrophilic properties, making it highly suitable for water treatment and biomolecule filtration applications.

The water uptake capacity of the membrane was evaluated using the gravimetric method. In this procedure, the membrane was immersed in deionized water for 24 h, after which its wet weight was measured. Subsequently, the membrane was oven-dried at 60 °C for 24 h, and the dry weight was recorded. The w represents the water uptake percentage, while W_w and W_d denote the weights of the wet and dry membranes, respectively (g).

3.3 Membrane performance

3.3.1 Effect of PDA coating on the membrane

Fig. 3 presents the integration of PDA into the membrane matrix offers a promising strategy for improving membrane performance in filtration processes, particularly in terms of flux and rejection efficiency. As a derivative of dopamine, PDA exhibits hydrophilic properties, which modify the membrane surface, enhance water interaction, and improve fouling resistance [31]. This study explores the effects of incorporating PDA at concentrations of 0.5% m/m, 1% m/m, and 1.5% m/m to determine the optimal concentration for maximizing membrane performance. The results indicate that the addition of PDA increases membrane flux, with the most significant improvements observed at 1% m/m and 1.5% m/m concentrations. This enhancement in flux can be attributed to the hydrophilic nature of PDA, which strengthens the interaction between water and the membrane surface. At the lower concentration of 0.5% m/m, the increase in flux is more moderate, still outperforming membranes without PDA, but less pronounced compared to the 1% m/m and 1.5% m/m concentrations. At the 1.5% m/m PDA concentration, the membrane demonstrates the highest flux, due to the formation of a more effective PDA surface layer that reduces resistance to water flow. The denser PDA layer at this concentration optimizes permeability, allowing smoother water flow through the membrane and enhancing its long-term stability

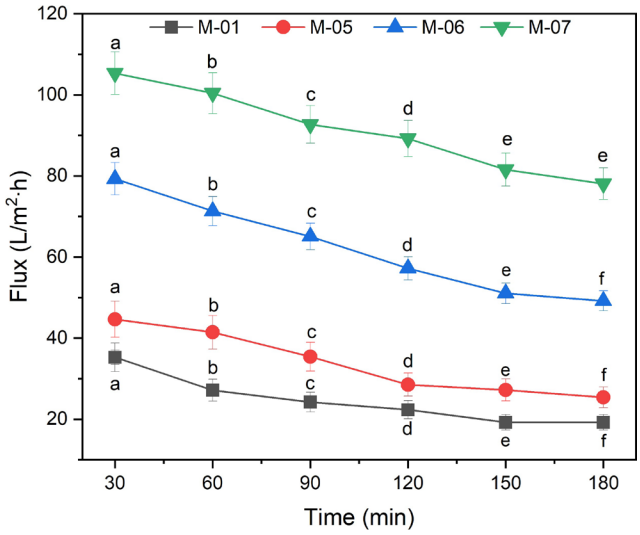

(a)

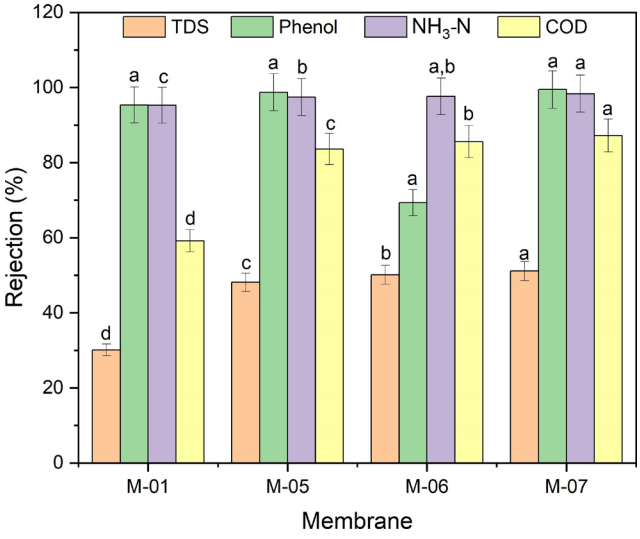

(b)

Fig. 3 (a) Flux and (b) rejection performance demonstrating the effect of polydopamine addition

and durability. Furthermore, membrane rejection reaches its highest value at the 1.5% m/m PDA concentration, attributed to the formation of a more compact and stable PDA layer on the membrane surface. This layer not only enhances the hydrophilic properties of the membrane but also strengthens the interactions between the membrane and contaminants, leading to improved separation efficiency.

3.3.2 Effect of pre-treatment on membrane performance

Pretreatment using bentonite adsorption and ozonation significantly reduces the concentration of the pollutants, such as TDS, phenol, ammonia, and COD in NR wastewater. As shown in Fig. 4 (a), activation of bentonite with 1 M HCl increases its adsorption capacity by expanding the pore structure, which facilitates the release of ions such as

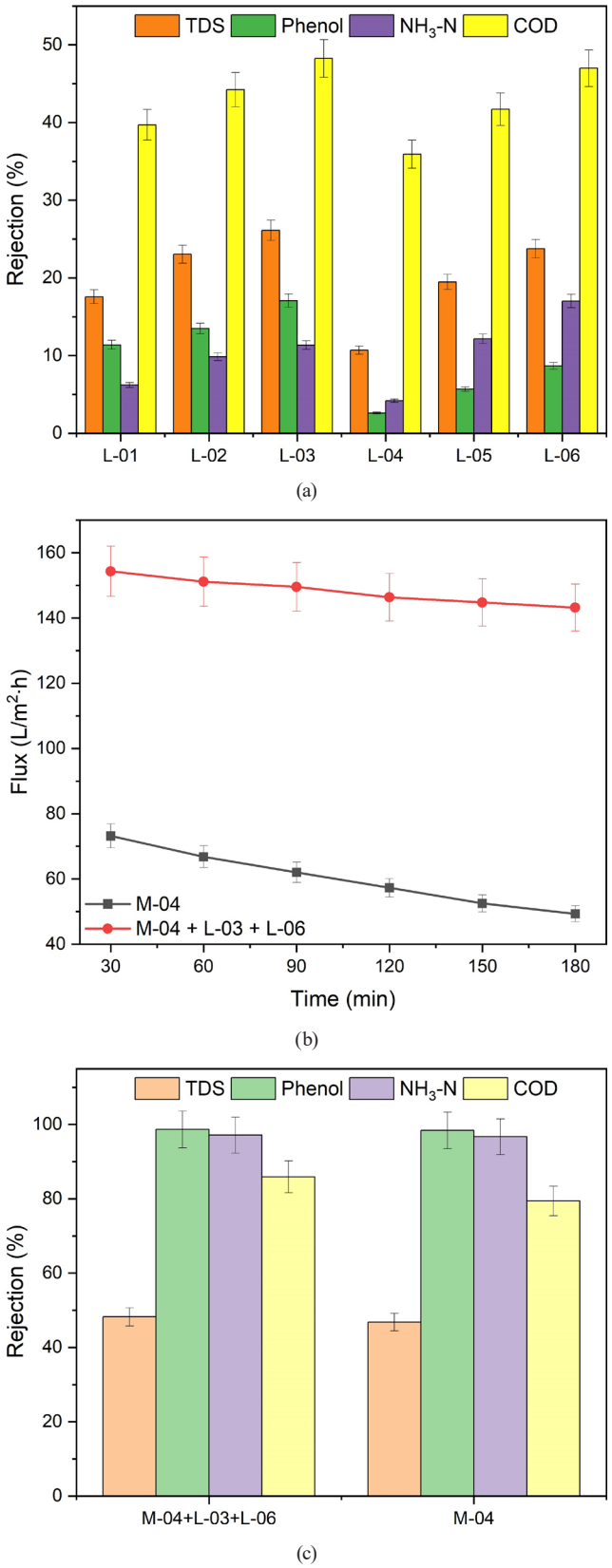

Fig. 4 (a) Adsorption–ozonation pretreatment (L-01: adsorption for 1 h, L-02: adsorption for 2 h, L-03: adsorption for 3 h, L-04: ozonation for 1 h, L-05: ozonation for 2 h, L-06: ozonation for 3 h), (b) flux values, and (c) rejection efficiency of pollutants with membrane integration and pretreatment

Al, Fe, and Mg, along with other impurities [32]. This activation results in a more physically active surface, enhancing pollutant adsorption. A 3 h contact time achieved pollutant reductions 26.13% for TDS, 17.08% for phenol, 11.35% for ammonia, and 48.24% for COD. Prolonged contact time allows greater diffusion and adsorption of pollutants, although the saturation of active sites may limit further adsorption. Ozonation pretreatment also demonstrates significant efficacy, with a 3 h process reducing TDS by 23.75%, phenol by 8.66%, ammonia by 17.02%, and COD by 46.98%. This improvement is attributed to the generation of highly reactive species, including $^{\bullet}OH$, $^{\bullet}O_2^-$, and ozone radicals, which facilitate the oxidation of complex organic compounds [33]. Extended ozonation further enhances ozone solubility and oxidation capacity, accelerating the breakdown of pollutants into simpler, more soluble by-products [34]. This effect is particularly evident in complex compounds like ammonia and phenol, which require extended oxidation periods for complete degradation. The combination of adsorption and ozonation demonstrates complementary efficacy, with adsorption capturing pollutants on the adsorbent surface, while ozonation decomposes compounds resistant to adsorption [35]. Experiments indicate optimal pollutant removal at 3 h durations for both processes (L-03 and L-06). L-03 (adsorption for 3 h) and L-06 (ozonation for 3 h) represent the pretreatment conditions with the best performance among the tested variables. Integrating these optimized pretreatment methods with membrane technology results in superior performance, as shown in Fig. 4 (b) and (c). Pretreatment reduces membrane fouling, stabilizes flux, and extends operational lifespan. This synergy minimizes the pollutant load during filtration, allowing membranes to effectively target residual pollutants, including complex organic compounds. The combined pretreatment and membrane approach significantly improves NH_3-N and COD rejection, highlighting its effectiveness in reducing fouling potential and enhancing pollutant removal. This integrated methodology offers a highly efficient and sustainable solution for rubber wastewater treatment, ensuring compliance with environmental standards while maintaining operational stability and reducing maintenance requirements.

3.3.3 Photodegradation performance and kinetic evaluation

Photodegradation has garnered significant attention as an effective method for wastewater treatment due to its ability to decompose organic pollutants into simpler compounds through photocatalytic mechanisms. Fig. 5 and

Table 5 present the photodegradation performance and the kinetic evaluation of three membrane types (M-01, M-04, M-07). Zero-order, pseudo-first-order, and modified Freundlich kinetic models were used to understand the material efficiency and the underlying reaction mechanisms. The results highlight significant differences in performance metrics, providing a deeper understanding of the strengths and limitations of each membrane.

Zero-order kinetic analysis revealed that M-01 exhibited the highest reaction rate constant (k_0 = 0.126 mg/L·min), surpassing M-04 (0.095 mg/L·min) and M-07 (0.092 mg/L·min). This higher rate constant indicates the superior photodegradation capability of M-01 under high-concentration conditions where active sites are saturated. Interestingly, M-01 achieved this performance despite the absence of incorporated photocatalytic materials. This result may be attributed

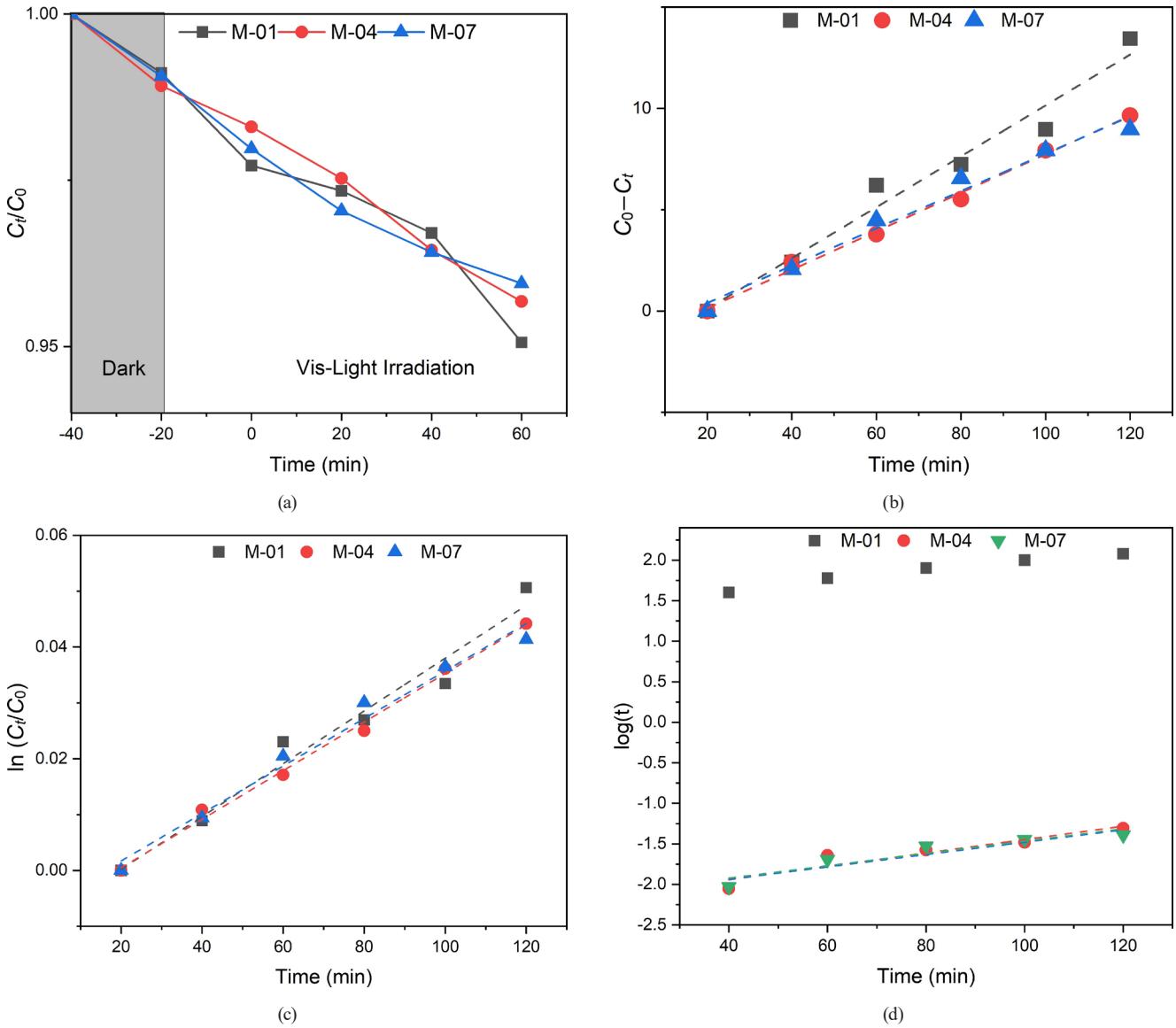

Fig. 5 (a) Photodegradation profiles of NR wastewater. Kinetic model fitting curves: (b) zero-order, (c) pseudo-first order, and (d) modified Freundlich models

Table 5 Model parameter estimates of photodegradation kinetics

Membranes	Zero-order kinetic		Pseudo-first order		Modified Freundlich		
	k_0 (mg/L·min)	R^2	k_1 (1/min)	R^2	k_F (1/min$^{1/m}$)	m	R^2
M-01	0.126	0.963	0.001	0.962	1.008	0.008	0.854
M-04	0.095	0.994	0.001	0.994	1.007	0.007	0.978
M-07	0.092	0.976	0.0009	0.977	1.001	0.001	0.839

to several intrinsic physicochemical attributes. Consequently, M-01 demonstrates accelerated initial photodegradation kinetics, even in the absence of added photocatalysts. In contrast, the incorporation of photocatalytic materials into M-04 and M-07, while designed to improve photocatalytic activity, may have introduced structural and optical drawbacks [36]. These include photocatalyst agglomeration and non-uniform dispersion, which can result in localized light scattering and shadowing effects. Such phenomena reduce the absorption of incident photons and hinder activation of the photocatalytically active domains, ultimately lowering the photodegradation efficiency [37, 38]. Thus, the slightly reduced rate constants for M-04 and M-07 are more likely indicative of practical morphological limitations rather than deficiencies in their inherent photocatalytic potential.

The pseudo-first-order kinetic model which is particularly suited to heterogeneous photocatalytic systems, where reaction rates are influenced by pollutant concentration, revealed that M-04 exhibited the highest rate constant (k_1 = 0.001 1/min) and an excellent linear fit (R^2 = 0.994), followed closely by M-07 (k_1 = 0.0009 1/min; R^2 = 0.977). These findings strongly support the notion that both M-04 and M-07 possess superior photocatalytic activity, likely attributed to their incorporation of TiO_2/WO_3-based nanohybrids, which effectively generate reactive oxygen species (ROS) under visible light [39].

Although M-01 showed a slightly higher zero-order rate constant (k_0 = 0.126 mg/L·min), this is not indicative of higher photocatalytic performance, but rather reflects non-catalytic photolysis and surface-driven adsorption at higher initial concentrations. The relatively lower R^2 value (0.963) compared to M-04 and M-07 also suggests a less consistent degradation mechanism. In contrast, the excellent fitting of M-04 in both zero-order (R^2 = 0.994) and pseudo-first-order models further confirms its consistent and efficient photocatalytic behavior.

The modified Freundlich model, which considers nonlinear adsorption on heterogeneous surfaces, also supports the enhanced performance of M-04. It demonstrated the best fit (R^2 = 0.978) with a relatively high Freundlich rate parameter (k_F = 1.007 $1/min^{1/m}$), suggesting a strong synergistic interaction between surface adsorption and photocatalytic degradation. While M-07 exhibited slightly lower adsorption capacity (k_F = 1.001), its consistent performance across all models affirms its reliability as an effective photocatalytic membrane, albeit requiring further optimization [40]. The performance differences among the membranes also highlight the role of material properties, such as bandgap energy, surface area, and oxygen-rich active site generation, in determining the photodegradation efficiency. Materials with narrower bandgaps exhibit higher photocatalytic activity under visible light, facilitating more efficient pollutant removal. For instance, M-04 membrane's superior bandgap characteristics likely contributed to its enhanced COD degradation via a synergistic combination of adsorption and photocatalysis. Moreover, performance variations among the membranes also reflect differences in material properties such as surface area, bandgap energy, and the generation of oxygen-rich active sites under irradiation. Membranes with narrower bandgaps, such as M-04, tend to exhibit enhanced photocatalytic activity under visible light due to more efficient charge carrier excitation. Furthermore, the formation of oxygen-rich sites within nanohybrid membranes enhances oxidative degradation, as these species serve as powerful oxidants in the breakdown of organic contaminants.

Meanwhile, M-01, which lacks photocatalytic additives, presented higher initial degradation rates under zero-order kinetics but lower fitting accuracy and reduced performance in the modified Freundlich model (R^2 = 0.854). This indicates that while M-01 may facilitate some degree of photolytic or adsorptive degradation, its overall photocatalytic contribution is limited. The comprehensive kinetic modeling confirms that M-04 and M-07 outperform M-01 in terms of true photocatalytic activity, driven by well-dispersed photocatalyst phases, optimized membrane, and favorable light absorption properties. These results underscore the critical role of photocatalyst incorporation and membrane design in enhancing pollutant removal efficiency in photocatalytic membrane systems.

3.3.4 Photocatalytic mechanism TiO_2/WO_3 membrane

The photocatalytic mechanism of the TiO_2/WO_3 membrane was systematically analyzed to evaluate its efficacy in degrading pollutants under visible light irradiation. As depicted in Fig. 6, the analysis focused on potential values relative to the normal hydrogen electrode (NHE). Both TiO_2 and WO_3 demonstrate strong light absorption at 450 nm, corresponding to direct band gaps of 3.07 eV and 2.01 eV, respectively. The conduction band (CB) and valence band (VB) positions of these materials were calculated using Mulliken electronegativity values and relevant equations [41].

$$E_{VB} = \chi_p - E_e - 0.5E_g \tag{6}$$

$$E_{CB} = E_{CB} + E_g \tag{7}$$

The χ represents the Mulliken electronegativity, E_e denotes the free electron energy on the hydrogen scale (4.5 eV),

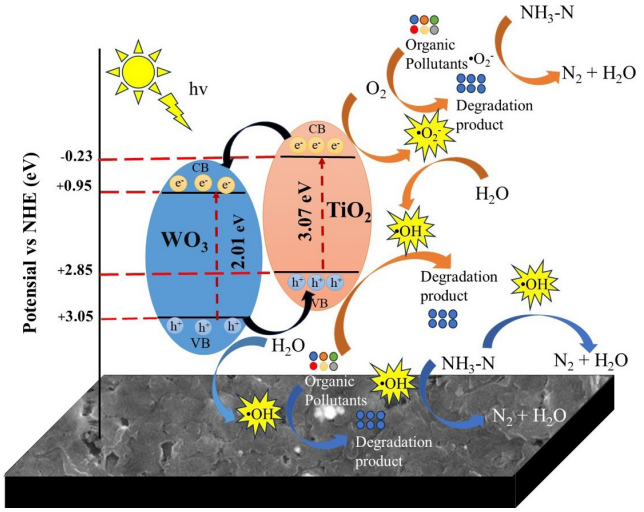

Fig. 6 The proposed photocatalytic mechanism of the TiO_2/WO_3 heterojunction

E_{VB} corresponds to the maximum energy of the VB, E_{CB} refers to the maximum energy of the CB, and E_g is the band gap energy. TiO_2 and MoS_2 exhibit electronegativity values 6.59 eV and 5.28 eV, respectively. The CB and VB potentials for WO_3 were determined to be +0.95 eV and +3.05 eV, while those for TiO_2 were −0.23 eV and +2.85 eV, relative to NHE. Under visible light irradiation, the membrane initiates a photocatalytic process in which incident photons excite electrons (e^-) in the VB of the photocatalyst, elevating them to the CB and leaving positively charged holes (h^+) in the VB [42]. This photon-induced charge carrier generation is essential for efficient photocatalysis. The TiO_2/WO_3 composite structure promotes effective charge separation and transport through strategic band alignment. Electrons in the CB of TiO_2 transfer to the CB of WO_3 due to the lower energy level of WO_3's CB, while holes migrate from the VB of WO_3 to the VB of TiO_2 because of the relative energy differences. This dual-directional charge carrier movement minimizes electron-hole recombination, a common challenge in photocatalysis that otherwise reduces efficiency. The separated charge carriers drive redox reactions that generate ROS, critical for pollutant degradation. Electrons in the CB of TiO_2 interact with molecular oxygen to produce superoxide radicals ($^\bullet O_2^-$), which subsequently react with water to form hydroxyl radicals ($^\bullet OH$). Simultaneously, holes in the VB of WO_3 oxidize water or hydroxide ions (OH^-) to produce additional hydroxyl radicals. These ROS are instrumental in decomposing complex organic pollutants and NH_3-N into environmentally benign products such as CO_2, N_2, and H_2O [43]. While the CB of WO_3 cannot directly reduce oxygen to $^\bullet O_2^-$ due to its higher potential (+0.95 eV) and the VB of TiO_2 cannot oxidize water to generate $^\bullet OH$ radicals, the synergistic interaction between TiO_2 and WO_3 overcomes these individual limitations. This interaction facilitates continuous ROS generation, enhancing pollutant degradation and improving the membrane permeability and pollutant rejection capabilities. The integration of TiO_2 and WO_3 into the membrane system represents a significant advancement in water treatment technologies, leveraging visible light-driven photocatalysis to achieve high efficiency and effectiveness in pollutant degradation. The photocatalytic reactions, outlined in Eqs. (11)–(38), provide a detailed understanding of ROS generation and their role in pollutant removal.

$$TiO_2 + hv \rightarrow h^+(TiO_2) + e^-(TiO_2) \quad (8)$$

$$e^-(TiO_2) + O_2 \rightarrow TiO_2 + {}^\bullet O_2^- \quad (9)$$

$$O_2 + 2H^+ + 2e^-(TiO_2) \rightarrow H_2O_2 \quad (10)$$

$$H_2O + e^- \rightarrow {}^\bullet OH + H^+ \quad (11)$$

The generation of holes in the VB of WO_3 under visible light irradiation.

$$WO_3 + hv \rightarrow h^+(WO_3) + e^-(WO_3) \quad (12)$$

$$h^+(WO_3) + OH^- + H^+ \rightarrow WO_3 + {}^\bullet OH + H^+ \quad (13)$$

The photodegradation reactions of pollutants are:

$$^\bullet OH + \text{pollutant organic} \rightarrow \text{degradation by-products } (CO_2 + H_2O + \text{other micromolecules}) \quad (14)$$

$$^\bullet O_2^- + \text{pollutant organic} \rightarrow \text{degradation by-products } (CO_2 + H_2O + \text{other micromolecules}). \quad (15)$$

The NH_3-N degradation reactions are:

$$NH_4^+ + 2OH^- \rightarrow NO_2^- + 3H_2 \quad (16)$$

$$2NO_2^- + O_2 \rightarrow 2NO_3^- \quad (17)$$

$$NO_3^- + 2H^+ + 2e^- \rightarrow ON_2^- + H_2O \quad (18)$$

$$NO_3^- + 10H^+ + 8e^- \rightarrow NH_4^+ + 3H_2O \quad (19)$$

$$2NO_3^- + 12H^+ + 10e^- \rightarrow 2N_2^- + 3H_2O. \quad (20)$$

3.3.5 Membrane stability

The stability of the membranes was evaluated by examining the reduction in normalized flux and the effectiveness of pollutant removal under both dark and visible light irradiation conditions, as shown in Fig. 7. Over five cycles, all membrane types demonstrated a gradual decline in normalized flux (J/J_0), indicating their vulnerability to fouling. M-07 membrane exhibited the highest stability, with the least flux reduction. In contrast, the M-01 membrane showed the greatest reduction, which can likely be attributed to variations in its surface and structural properties. The incorporation of TiO_2/WO_3 photocatalytic materials and PDA coating notably enhanced the membrane structural integrity by increasing porosity, which promoted the formation of non-clogged water channel. This design effectively minimized clogging and ensured a consistent production of ROS throughout multiple cycles, thereby supporting the membrane's long-term operational efficiency in water treatment [44]. Furthermore, the addition of photocatalytic materials improved the hydrophilicity of the membranes, as demonstrated by a reduction in contact angle, which enhanced water affinity and reduced fouling deposition on the membrane surface. While backwashing was effective in restoring flux for all membranes, a slight decrease in recovery rates was observed with each subsequent cycle, indicating some degree of irreversible fouling or material degradation [45]. The pollutant removal efficiency remained consistently high, with all membranes maintaining removal rates above 90% under visible light conditions across all cycles. This stability highlights the

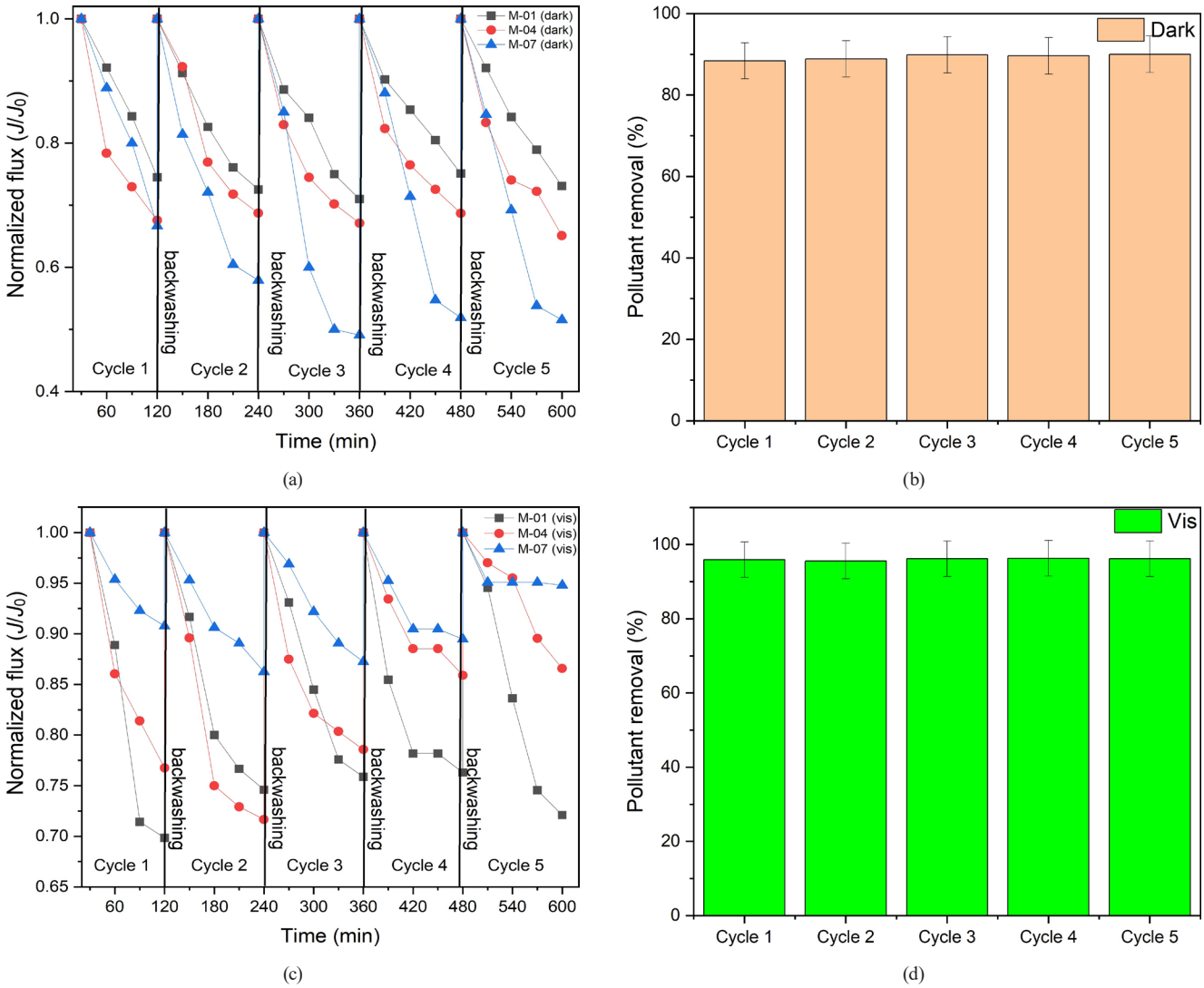

Fig. 7 Cycle test results of membranes: (a) normalized flux under dark conditions, (b) pollutant removal under dark conditions, (c) normalized flux under visible light irradiation, (d) pollutant removal under visible light irradiation

membranes' exceptional separation performance, with minimal influence from operating conditions on their pollutant rejection capabilities. Visible light irradiation played a critical role in enhancing both flux stability and pollutant rejection, underscoring the positive impact of photocatalysis on membrane performance. Overall, M-07 membrane displayed the most promising outcomes, characterized by superior flux retention, efficient backwash recovery, and consistent pollutant removal throughout all cycles.

3.3.6 Fouling evaluation membrane

To further assess the fouling resistance of the TiO_2/WO_3 composite membrane, a comprehensive evaluation was conducted. Fig. 8 (a) presents a comprehensive analysis of the antifouling performance of the M-07 membrane, which represents the optimal formulation incorporating both TiO_2/WO_3 photocatalysts and 1.5% m/m PDA. Fig. 8 illustrates key fouling-related parameters, including the flux recovery ratio (FRR), total fouling resistance (R_T), reversible fouling resistance (R_r), and irreversible fouling resistance (R_{ir}), under both visible light and dark conditions. These parameters are essential in evaluating the membrane resilience to fouling and its ability to recover performance after filtration cycles. The FRR reflects the extent to which the membrane can restore its initial water flux after a cleaning process, with higher FRR values indicating superior fouling reversibility and membrane reusability. R_T quantifies the overall decline in flux resulting from the accumulation of foulants on or within the membrane matrix. This resistance can be further delineated into reversible and irreversible components. The R_r corresponds to the fraction of fouling that can be effectively removed through physical cleaning methods such as backflushing, implying weakly bound foulants. In contrast, the R_{ir} represents the fouling that persists despite cleaning efforts and often necessitates chemical treatment, typically due to the strong adhesion or entrapment of pollutants within the membrane pores. Membranes subjected to visible light irradiation exhibited a lower R_T and a higher FRR, indicating that visible light exposure effectively reduced fouling and improved the membrane performance. In contrast, under dark conditions, the membranes demonstrated lower fouling resistance, with the R_r value surpassing R_{ir}, further confirming the excellent antifouling properties of the membrane. This enhanced performance is attributed to the superior hydrophilicity of the membrane, which promotes the spreading of water across the surface and inhibits the accumulation of foulants. This

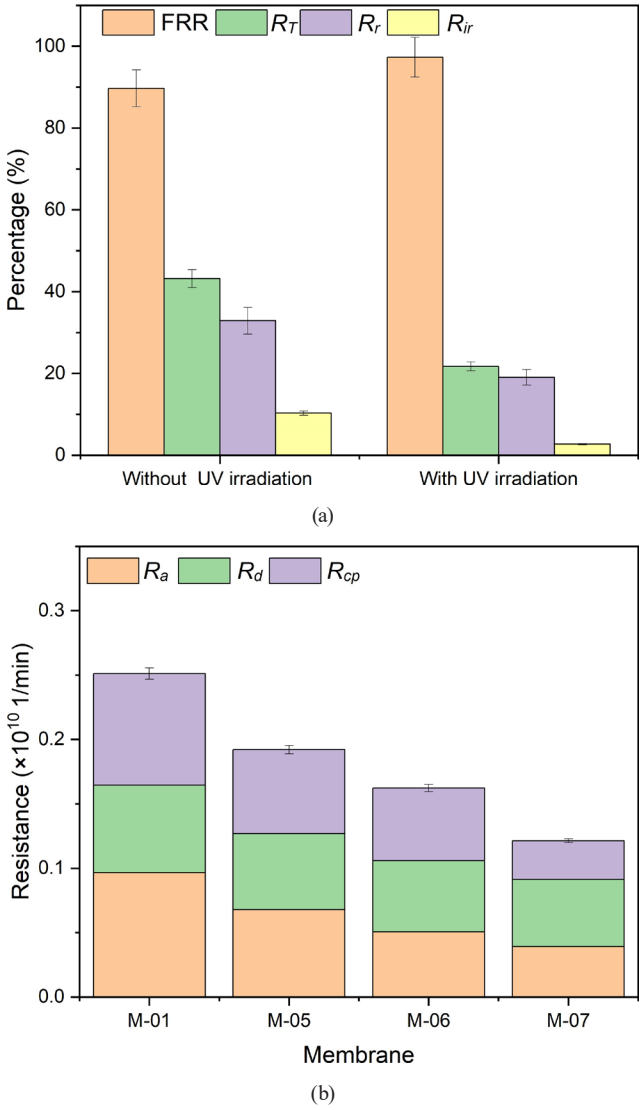

Fig. 8 (a) Fouling percentage of flux recovery ratio, (b) fouling resistance of membrane

is supported by the presence of hydroxyl (−OH) groups on the membrane, as revealed by FTIR analysis, which contributes to the membrane's enhanced hydrophilic characteristics. The increased hydrophilicity reduces the interaction between the membrane surface and specific foulant molecules, thereby improving fouling resistance. The comparative analysis of results under visible light irradiation versus dark conditions emphasizes the significant role of light in activating the TiO_2/WO_3 composite incorporated into the membrane. The photocatalytic activity of TiO_2/WO_3 under visible light likely facilitates the degradation of organic foulants, thus reducing their deposition on the membrane surface and further enhancing the antifouling performance. This activation of TiO_2/WO_3 under visible light improves the membrane's ability to resist fouling by breaking down pollutants before they can

adhere to the membrane surface. The inclusion of PDA further improves fouling resistance, as evidenced by a substantial reduction in fouling deposition resistance (R_d). This enhancement can be attributed to the photocatalytic degradation of foulants on the membrane surface, which prevents the accumulation of contaminants. Membranes modified with 1.5% m/m PDA concentration exhibited the lowest fouling resistance, reflecting superior antifouling properties. According to Davari et al. [46], PDA enhances nanoparticle binding stability, thereby improving membrane functionality. Additionally, PDA has been shown to facilitate pollutant removal and offer protection against fouling. The PDA coating not only increases the membrane selectivity but also provides an additional layer of antifouling defense. Notably, longer coating durations result in thicker PDA layers, which further enhance the membrane resistance to water absorption and improve its overall fouling resistance. In conclusion, the incorporation of TiO_2/WO_3 photocatalytic materials and the PDA coating enhances both the fouling resistance and the overall performance of the membrane. The synergistic effects of visible light-driven photocatalysis and the hydrophilic properties of the membrane, combined with the protective and stabilizing role of the PDA coating, lead to a substantial reduction in fouling deposition.

3.4 Comparison with previous studies

The performance of the PVDF/TiO_2/WO_3/PDA ultrafiltration membrane developed in this study was evaluated in comparison to other photocatalytic membranes reported in the literature for the treatment of NR wastewater. Table 6 [47–50] highlights the key differences in membrane configurations, nanoparticle compositions, feedwater properties, and resulting flux values. This analysis emphasizes the superior performance of the current membrane, particularly in achieving higher flux and pollutant removal efficiencies, including NH_3-N, phenol, COD, and TDS. The advancements in the current membrane design are attributed to the synergistic effects of the TiO_2/WO_3/PDA composite. The incorporation of WO_3 enhances visible-light absorption, while PDA improves the hydrophilicity and antifouling properties of the membrane. These features collectively contribute to the enhanced flux and pollutant rejection efficiencies observed in this study.

4 Conclusion

The PDA coating improved the adhesion and dispersion of photocatalyst particles, leading to superior membrane performance. Comprehensive characterization confirmed that the PVDF-TiO_2-WO_3/PDA membrane exhibited improved mechanical properties, porosity, hydrophilicity, and pollutant rejection. The membrane achieved remarkable rejection rates for ammonia (98.22%), phenol (99.39%), COD (87.18%), and TDS (51.06%), with a flux value of 154.32 L/m^2·h after pretreatment. The incorporation of TiO_2-WO_3 nanoparticles enhanced photocatalytic degradation under visible light, while the PDA coating ensured high selectivity and stability. Kinetic analysis indicated that the photocatalytic activity followed a zero-order reaction model. Notably, the membrane maintained stable performance over five operational cycles, showing resilience against fouling and swelling.

Acknowledgement

This project is financially supported by the grant of Research Professor (RP UNDIP) No.120-31/UN7.6.1/PP/2025. Special gratitude to the Institute for Research and Community Services, Diponegoro University (LPPM UNDIP) for the assistance during the completion of this project.

Table 6 Comparison of the photocatalytic membranes

Membrane	Nanoparticles	Feed water	Flux (L/m^2·h)	Features	Ref.
PES/Nanofiltration	TiO_2	NR wastewater	80	Organic removal 95.83%, salt 72.40%, NH_3-N 95.66%.	[47]
PSf/Nanofiltration	TiO_2/GO	NR wastewater	16.29	Organic removal ~80%, ammonia removal ~90%	[48]
PSf/Nanofiltration	ZnO-MnO_2@SiO_2	NR wastewater	27.31	TDS 73.26% Phenol 68.33% COD 78.92% NH_3-N 75.69%	[49]
PVDF/Nanofiltration	MoS_2@WO_3	NR wastewater	63.69	COD 97.04%, TDS 90.63% NH_3-N 95.64%	[50]
PVDF/Ultrafiltration	TiO_2/WO_3/PDA	NR wastewater	154.32	NH_3-N 98.22% Phenol 99.39% COD 87.18%, TDS 51.06%	[Present study]

References

[1] Obaideen, K., Shehata, N., Sayed, E. T., Abdelkareem, M. A., Mahmoud, M. S., Olabi, A. G. "The role of wastewater treatment in achieving sustainable development goals (SDGs) and sustainability guideline", Energy Nexus, 7, 100112, 2022. https://doi.org/10.1016/j.nexus.2022.100112

[2] Husaini, A., Fahrezi, D. D., Arbavella, M. A., Sadewa, N. P. "Analisis Ekspor Komoditi Karet di Indonesia Terhadap Perdagangan Internasional 2016-2020" (Analysis of Indonesia's Rubber Commodity Exports in Relation to International Trade (2016–2020)), Jurnal Economica, 2(2), pp. 439–445, 2023. (in Indonesian) https://doi.org/10.55681/economina.v2i2.320

[3] Kusworo, T. D., Kumoro, A. C., Aryanti, N., Utomo, D. P. "Removal of organic pollutants from rubber wastewater using hydrophilic nanocomposite rGO-ZnO/PES hybrid membranes", Journal of Environmental Chemical Engineering, 9(6), 106421, 2021. https://doi.org/10.1016/j.jece.2021.106421

[4] Zhu, D., Ge, C., Sun, Y., Yu, H., Wang, J., Sun, H. "Identification of organic pollutants and heavy metals in natural rubber wastewater and evaluation its phytotoxicity and cytogenotoxicity", Chemosphere, 349, 140503, 2024. https://doi.org/10.1016/j.chemosphere.2023.140503

[5] Xie, X., Wang, L., Wei, J., He, H., Guo, Z., Wang, C., Wen, X., Song, Y. "Progress in ceramic membrane coupling ozonation process for water and wastewater treatment: A critical review", Chemical Engineering Journal, 493, 152475, 2024. https://doi.org/10.1016/j.cej.2024.152475

[6] Gidstedt, S., Betsholtz, A., Falås, P., Cimbritz, M., Davidsson, Å., Micolucci, F., Svahn, O. "A comparison of adsorption of organic micropollutants onto activated carbon following chemically enhanced primary treatment with microsieving, direct membrane filtration and tertiary treatment of municipal wastewater", Science of The Total Environment, 811, 152225, 2022. https://doi.org/10.1016/j.scitotenv.2021.152225

[7] Kamalesh, R., Karishma, S., Saravanan, A., Yaashikaa, P. R. "Emerging breakthroughs in membrane filtration techniques and their application in agricultural wastewater treatment: Reusability aspects", Sustainable Chemistry for the Environment, 8, 100183, 2024. https://doi.org/10.1016/j.scenv.2024.100183

[8] Momina, Ahmad, K. "Feasibility of the adsorption as a process for its large scale adoption across industries for the treatment of wastewater: Research gaps and economic assessment", Journal of Cleaner Production, 388, 136014, 2023. https://doi.org/10.1016/j.jclepro.2023.136014

[9] Zhang, J., Yu, H., Quan, X., Chen, S., Zhang, Y. "Ceramic membrane separation coupled with catalytic ozonation for tertiary treatment of dyestuff wastewater in a pilot-scale study", Chemical Engineering Journal, 301, pp. 19–26, 2016. https://doi.org/10.1016/j.cej.2016.04.148

[10] Krishnamoorthy, M., Mohamed, M. A., Kaus, N. H. M., Yusoff, S. F. M. "Adsorption and photocatalytic degradation of cationic dyes over bismuth ferrite (BFO) intercalated on liquid natural rubber-based hydrogel compound", Journal of Industrial and Engineering Chemistry, 116, pp. 447–464, 2022. https://doi.org/10.1016/j.jiec.2022.09.035

[11] Chang, Z. H., Lyly, L. H. T., Sum, J. Y. "A review on membrane separation in natural rubber processing: Concentration, recovery and treatment", Chemical Engineering and Processing - Process Intensification, 193, 109541, 2023. https://doi.org/10.1016/j.cep.2023.109541

[12] Shehata, N., Egirani, D., Olabi, A. G., Inayat, A., Abdelkareem, M. A., Chae, K.-J., Sayed, E. T. "Membrane-based water and wastewater treatment technologies: Issues, current trends, challenges, and role in achieving sustainable development goals, and circular economy", Chemosphere, 320, 137993, 2023. https://doi.org/10.1016/j.chemosphere.2023.137993

[13] Nasrollahi, N., Ghalamchi, L., Vatanpour, V., Khataee, A. "Photocatalytic-membrane technology: a critical review for membrane fouling mitigation", Journal of Industrial and Engineering Chemistry, 93, pp. 101–116, 2021. https://doi.org/10.1016/j.jiec.2020.09.031

[14] Kang, G.-d., Cao, Y.-m. "Application and modification of poly(vinylidene fluoride) (PVDF) membranes – A review", Journal of Membrane Science, 463, pp. 145–165, 2014. https://doi.org/10.1016/j.memsci.2014.03.055

[15] Hirota, M., Sugita, Y., Ishijima, M., Ikeda, T., Saruta, J., Maeda, H., Ogawa, T. "UV photocatalytic activity of titanium dioxide (TiO_2) surface contaminated with bacterial biofilm: Implications for photo-restoration of osteoconductivity", Materials Today Advances, 12, 100182, 2021. https://doi.org/10.1016/j.mtadv.2021.100182

[16] Murillo-Sierra, J. C., Hernández-Ramírez, A., Hinojosa-Reyes, L., Guzmán-Mar, J. L. "A review on the development of visible light-responsive WO_3-based photocatalysts for environmental applications", Chemical Engineering Journal Advances, 5, 100070, 2021. https://doi.org/10.1016/j.ceja.2020.100070

[17] Li, H., Yin, D., Li, W., Tang, Q., Zou, L., Peng, Q. "Polydopamine-based nanomaterials and their potentials in advanced drug delivery and therapy", Colloids and Surfaces B: Biointerfaces, 199, 111502, 2021. https://doi.org/10.1016/j.colsurfb.2020.111502

[18] Kusworo, T. D., Yulfarida, M., Kumoro, A. C., Sumardiono, S., Djaeni, M., Kurniawan, T. A., Othman, M. H. D., Budiyono, B. "A highly durable and hydrophilic PVDF-MoS_2/WO_3-PVA membrane with visible light driven self-cleaning performance for pollutant-burdened natural rubber wastewater treatment", Journal of Environmental Chemical Engineering, 11(2), 109583, 2023. https://doi.org/10.1016/j.jece.2023.109583

[19] Kusworo, T. D., Puspa, M. B., Kumoro, A. C., Sutapa, I. D. A., Dalanta, F., Utomo, D. P. "Manufacture and performance assessment of PVDF-La@TiO_2 Photocatalyst implanted membrane for efficient produced water treatment via ozonation-adsorption process under visible-light exposure", Journal of Water Process Engineering, 67, 106179, 2024. https://doi.org/10.1016/j.jwpe.2024.106179

[20] Kaur, B., Choudhary, R., Sharma, G., Brar, L. K. "Sustainable and effective microorganisms method for wastewater treatment", Desalination and Water Treatment, 319, 100419, 2024. https://doi.org/10.1016/j.dwt.2024.100419

[21] Wei, Q., Feng, S., Zhang, Z., Liu, L., Wu, L. "A high-protein retained PES hemodialysis membrane with tannic acid as a multifunctional modifier", Colloids and Surfaces B: Biointerfaces, 220, 112921, 2022. https://doi.org/10.1016/j.colsurfb.2022.112921

[22] Tubío, C. R., Guitián, F., Salgueiro, J. R., Gil, A. "Anatase and rutile TiO_2 monodisperse microspheres by rapid thermal annealing: A method to avoid sintering at high temperatures", Materials Letters, 141, pp. 203–206, 2015. https://doi.org/10.1016/j.matlet.2014.11.063

[23] Sukarman, Kristiawan, B., Khoirudin, Abdulah, A., Enoki, K., Wijayanta, A. T. "Characterization of TiO_2 nanoparticles for nanomaterial applications: Crystallite size, microstrain and phase analysis using multiple techniques", Nano-Structures & Nano-Objects, 38, 101168, 2024. https://doi.org/10.1016/j.nanoso.2024.101168

[24] Preethi, L. K., Mathews, T., Nand, M., Jha, S. N., Gopinath, C. S., Dash, S. "Band alignment and charge transfer pathway in three phase anatase-rutile-brookite TiO_2 nanotubes: An efficient photocatalyst for water splitting", Applied Catalysis B: Environmental, 218, pp. 9–19, 2017. https://doi.org/10.1016/j.apcatb.2017.06.033

[25] Zhai, Y., Yang, J. "Fabrication and modification of PVDF membrane by PDA@ZnO for enhancing hydrophilic and antifouling property", Arabian Journal of Chemistry, 16(11), 105206, 2023. https://doi.org/10.1016/j.arabjc.2023.105206

[26] Abd El-Aziz, A. M., Afifi, M. "Influence the β-PVDF phase on structural and elastic properties of PVDF/PLZT composites", Materials Science and Engineering: B, 301, 117152, 2024. https://doi.org/10.1016/j.mseb.2023.117152

[27] Samuel, O., Othman, M. H. D., Kamaludin, R., Sinsamphanh, O., Abdullah, H., Puteh, M. H., Kurniawan, T. A. "WO_3–based photocatalysts: A review on synthesis, performance enhancement and photocatalytic memory for environmental applications", Ceramics International, 48(5), pp. 5845–5875, 2022. https://doi.org/10.1016/j.ceramint.2021.11.158

[28] Wang, Z., Wei, H., He, Z., Liu, X., Chen, L., Tao, W.-Q. "Effects of Cassie-Wenzel wetting transition on two-phase flow in porous media", International Communications in Heat and Mass Transfer, 146, 106931, 2023. https://doi.org/10.1016/j.icheatmasstransfer.2023.106931

[29] Wang, H., Jing, L., Varamesh, A., Yan, Y., Zhang, H., Gao, Q., Hu, J. "Application of Polydopamine-Based Photocatalysts in Energy and Environmental Systems", Photocatalysis: Research and Potential, 1(3), 10007, 2023. https://doi.org/10.70322/prp.2024.10007

[30] Ye, N., Wang, J., Yan, X., Sha, D., Chen, M., Zhou, C., Wang, D., Yuan, X., Cheng, X., Zu, J. "Novel $Cs_x WO_3/TiO_2$ Microspheres as Enhanced Visible Light Photocatalysts for Dye Pollutant Treatments", Journal of Nanoscience and Nanotechnology, 18(8), pp. 5485–5492, 2018. https://doi.org/10.1166/jnn.2018.15438

[31] Chang, Z. H., Lyly, L. H. T., Teow, Y. H., Yeap, S. P., Sum, J. Y. "Insight into polydopamine coating on microfiltration membrane with controlled surface pore size for enhanced membrane rejection", Polymer, 287, 126446, 2023. https://doi.org/10.1016/j.polymer.2023.126446

[32] Toor, M., Jin, B., Dai, S., Vimonses, V. "Activating natural bentonite as a cost-effective adsorbent for removal of Congo-red in wastewater", Journal of Industrial and Engineering Chemistry, 21, pp. 653–661, 2015. https://doi.org/10.1016/j.jiec.2014.03.033

[33] Das, P. P., Dhara, S., Samanta, N. S., Purkait, M. K. "Advancements on ozonation process for wastewater treatment: A comprehensive review", Chemical Engineering and Processing - Process Intensification, 202, 109852, 2024. https://doi.org/10.1016/j.cep.2024.109852

[34] Zhang, H., Li, S., Zhang, C., Ren, X., Zhou, M. "A critical review of ozone-based electrochemical advanced oxidation processes for water treatment: Fundamentals, stability evaluation, and application", Chemosphere, 365, 143330, 2024. https://doi.org/10.1016/j.chemosphere.2024.143330

[35] Loganathan, P., Kandasamy, J., Jamil, S., Ratnaweera, H., Vigneswaran, S. "Ozonation/adsorption hybrid treatment system for improved removal of natural organic matter and organic micropollutants from water – A mini review and future perspectives", Chemosphere, 296, 133961, 2022. https://doi.org/10.1016/j.chemosphere.2022.133961

[36] Le, T. M. H., Wang, Y.-N., Li, C., Wang, R., Sairiam, S. "Durable PVDF photocatalytic membranes with TiO_2@PDA incorporated into/onto for dye degradation under visible-light", Chemical Engineering Journal, 499, 156215, 2024. https://doi.org/10.1016/j.cej.2024.156215

[37] Pellegrino, F., Pellutiè, L., Sordello, F., Minero, C., Ortel, E., Hodoroaba, V.-D., Maurino, V. "Influence of agglomeration and aggregation on the photocatalytic activity of TiO_2 nanoparticles", Applied Catalysis B: Environmental, 216, pp. 80–87, 2017. https://doi.org/10.1016/j.apcatb.2017.05.046

[38] Tolosana-Moranchel, A., Pecharromán, C., Faraldos, M., Bahamonde, A. "Strong effect of light scattering by distribution of TiO_2 particle aggregates on photocatalytic efficiency in aqueous suspensions", Chemical Engineering Journal, 403, 126186, 2021. https://doi.org/10.1016/j.cej.2020.126186

[39] Ezzati, R., Azizi, M., Ezzati, S. "A theoretical approach for evaluating the contributions of pseudo-first-order and pseudo-second-order kinetics models in the Langmuir rate equation", Vacuum, 222, 113018, 2024. https://doi.org/10.1016/j.vacuum.2024.113018

[40] Zhao, C., Zhang, W., Zhang, Y., Yang, Y., Guo, D., Liu, W., Liu, L. "Influence of multivalent background ions competition adsorption on the adsorption behavior of azo dye molecules and removal mechanism: Based on machine learning, DFT and experiments", Separation and Purification Technology, 341, 126810, 2024. https://doi.org/10.1016/j.seppur.2024.126810

[41] Dalanta, F., Kusworo, T. D., Aryanti, N. "Synthesis, characterization, and performance evaluation of UV light-driven Co-TiO_2@SiO_2 based photocatalytic nanohybrid polysulfone membrane for effective treatment of petroleum refinery wastewater", Applied Catalysis B: Environmental, 316, 121576, 2022. https://doi.org/10.1016/j.apcatb.2022.121576

[42] Chakravorty, A., Roy, S. "A review of photocatalysis, basic principles, processes, and materials", Sustainable Chemistry for the Environment, 8, 100155, 2024.
https://doi.org/10.1016/j.scenv.2024.100155

[43] Dong, C., Fang, W., Yi, Q., Zhang, J. "A comprehensive review on reactive oxygen species (ROS) in advanced oxidation processes (AOPs)", Chemosphere, 308, 136205, 2022.
https://doi.org/10.1016/j.chemosphere.2022.136205

[44] van Zwieten, R., van de Laar, T., Sprakel, J., Schroën, K. "From cooperative to uncorrelated clogging in cross-flow microfluidic membranes", Scientific Reports, 8(1), 5687, 2018.
https://doi.org/10.1038/s41598-018-24088-6

[45] Chang, H., Liang, H., Qu, F., Liu, B., Yu, H., Du, X., Li, G., Snyder, S. A. "Hydraulic backwashing for low-pressure membranes in drinking water treatment: A review", Journal of Membrane Science, 540, pp. 362–380, 2017.
https://doi.org/10.1016/j.memsci.2017.06.077

[46] Davari, S., Omidkhah, M., Salari, S. "Role of polydopamine in the enhancement of binding stability of TiO_2 nanoparticles on polyethersulfone ultrafiltration membrane", Colloids and Surfaces A: Physicochemical and Engineering Aspects, 622, 126694, 2021.
https://doi.org/10.1016/j.colsurfa.2021.126694

[47] Kusworo, T. D., Kumoro, A. C., Utomo, D. P., Kusumah, F. M., Pratiwi, M. D. "Performance of the Crosslinked PVA Coated PES-TiO_2 Nano Hybrid Membrane for the Treatment of Pretreated Natural Rubber Wastewater Involving Sequential Adsorption – Ozonation Processes", Journal of Environmental Chemical Engineering, 9(2), 104855, 2021.
https://doi.org/10.1016/j.jece.2020.104855

[48] Kusworo, T. D., Susanto, H., Aryanti, N., Rokhati, N., Widiasa, I. N., Al-Aziz, H., Utomo, D. P., Masithoh, D., Kumoro, A. C. "Preparation and characterization of photocatalytic PSf-TiO_2/GO nanohybrid membrane for the degradation of organic contaminants in natural rubber wastewater", Journal of Environmental Chemical Engineering, 9(2), 105066, 2021.
https://doi.org/10.1016/j.jece.2021.105066

[49] Kusworo, T. D., Kumoro, A. C., Aryanti, N., Kurniawan, T. A., Dalanta, F., Alias, N. H. "Photocatalytic polysulfone membrane incorporated by ZnO-MnO_2@SiO_2 composite under UV light irradiation for the reliable treatment of natural rubber-laden wastewater", Chemical Engineering Journal, 451, 138593, 2023.
https://doi.org/10.1016/j.cej.2022.138593

[50] Kusworo, T. D., Kumoro, A. C., Yulfarida, M. "A new visible-light driven photocatalytic PVDF-MoS_2@WO_3 membrane for clean water recovery from natural rubber wastewater", Journal of Water Process Engineering, 52, 103522, 2023.
https://doi.org/10.1016/j.jwpe.2023.103522